Available online at www.sciencedirect.com

ScienceDirect

Advances in Climate Change Research xxx (xxxx) xxx

www.keaipublishing.com/en/journals/accr/

Water budgets in an arid and alpine permafrost basin: Observations from the High Mountain Asia

Qing-Feng WANG[a,b,1], Hui-Jun JIN[a,c,*], Dong-Liang LUO[a,1], Yu SHENG[a], Jun WEN[a,d], Chien-Lu PING[e], Mark H. CLARK[f], Qiang MA[a], Xiao-Ying JIN[c], Ji-Chun WU[a,b], Yu-Zhong YANG[a], Qiang LI[g], Raul D. ŞERBAN[a,h,i], Daqing YANG[j,k], Victor F. BENSE[a,l], Qing-Bai WU[a,b]

[a] *Key Laboratory of Cryospheric Science and Frozen Soil Engineering, Northwest Institute of Eco-Environment and Resources, Chinese Academy of Sciences, Lanzhou 730000, China*

[b] *Qinghai-Beiluhe Plateau Frozen Soil Engineering Safety National Observation and Research Station, Northwest Institute of Eco-Environment and Resources, Chinese Academy of Sciences, Lanzhou 730000, China*

[c] *School of Civil Engineering and Transportation, China–Russia Joint Laboratory of Cold Regions Engineering and Environment, and Permafrost Institute, Northeast Forestry University, Harbin 150040 China*

[d] *College of Atmospheric Science, Plateau Atmosphere and Environment Key Laboratory of Sichuan Province, Chengdu University of Information Technology, Chengdu 610225, China*

[e] *Agricultural and Forestry Experiment Station, University of Alaska Fairbanks, Palmer Research Center, Palmer 99645, USA*

[f] *USDA-Natural Resources Conservation Service, Palmer 99645, USA*

[g] *College of Water Conservancy and Hydropower Engineering, Gansu Agricultural University, Lanzhou 730070, China*

[h] *Institute for Alpine Environment, Eurac Research, Bolzano 39100, Italy*

[i] *Faculty of Agricultural, Environmental and Food Sciences, Free University of Bozen-Bolzano, Bolzano 39100, Italy*

[j] *Watershed Hydrology and Ecology Division, Environment and Climate Change Canada, Victoria V8S 3V3, Canada*

[k] *Institute of Tibetan Plateau Research, Chinese Academy of Sciences, Beijing 100101, China*

[l] *Hydrology and Quantitative Water Management Group, Department of Environmental Sciences, Wageningen University, Wageningen 6700, the Netherlands*

Received 20 May 2024; revised 10 September 2024; accepted 20 September 2024

Abstract

Ground freeze–thaw processes have significant impacts on infiltration, runoff and evapotranspiration. However, there are still critical knowledge gaps in understanding of hydrological processes in permafrost regions, especially of the interactions among permafrost, ecology, and hydrology. In this study, an alpine permafrost basin on the northeastern Qinghai–Tibet Plateau was selected to conduct hydrological and meteorological observations. We analyzed the annual variations in runoff, precipitation, evapotranspiration, and changes in water storage, as well as the mechanisms for runoff generation in the basin from May 2014 to December 2015. The annual flow curve in the basin exhibited peaks both in spring and autumn floods. The high ratio of evapotranspiration to annual precipitation (>1.0) in the investigated wetland is mainly due to the considerably underestimated 'observed' precipitation caused by the wind-induced instrumental error and the neglect of snow sublimation. The stream flow from early May to late October probably came from the lateral discharge of subsurface flow in alpine wetlands. This study can provide data support and validation for hydrological model simulation and prediction, as well as water resource assessment, in the upper Yellow River Basin, especially for the headwater area. The results also provide case support for permafrost hydrology modeling in ungauged or poorly gauged watersheds in the High Mountain Asia.

Keywords: Water budget; Runoff; Freeze–thaw processes; Active layer; Permafrost basin; Alpine wetland

* Corresponding author. School of Civil Engineering and Transportation, Northeast Forestry University, Harbin 150040 China.
E-mail address: hjjin@nefu.edu.cn (JIN H.-J.).

Peer review under responsibility of National Climate Centre (China Meteorological Administration).

[1] The authors contributed equally.

https://doi.org/10.1016/j.accre.2024.09.005

Please cite this article as: WANG, Q.-F et al., Water budgets in an arid and alpine permafrost basin: Observations from the High Mountain Asia, Advances in Climate Change Research, https://doi.org/10.1016/j.accre.2024.09.005

1. Introduction

As the main body of the High Mountain Asia (HMA), also known as the Third Pole, the Qinghai−Tibet Plateau (QTP) is the sources of more than 10 large Asian rivers, such as the Yangtze River, Yellow River, Mekong River, and Indus River, and is often hailed as the Water Towers of Asia due to its huge water resources in liquid and solid forms (Yao et al., 2019a).

Permafrost on the QTP covers an areal extent of ~1.06 million km^2, accounting for >40% of the total plateau area (Ran et al., 2021; Zou et al., 2017). Over the last 50 years, the overall QTP has become warmer and wetter. In 1960−2012, the warming rate of mean annual air temperature on the QTP was approximately twice of the global average (Chen et al., 2015; Yao et al., 2022), with the largest warming rate in the continuous permafrost regions on the northern QTP (Yang et al., 2014). Consequently, permafrost has been widely degrading (Zhao et al., 2024; Cheng and Jin, 2013; Ding et al., 2019; Jin et al., 2000; Li et al., 2008). This affects not only the water resource supply for ~1.6 billion people in East and South Asia (Immerzeel et al., 2020), but also the westerlies−monsoon interactions (An et al., 2001; Chen et al., 2020). The westerlies−monsoon interactions would eventually affect regional to global climate changes and water cycles *via* three-pole coordinated changes in the atmosphere and hydrosphere (Yao et al., 2019b; Li et al., 2020a).

Ground freeze−thaw processes have significant impacts on infiltration, runoff, and evapotranspiration, and are crucial in regulating the hydrological processes in cold regions (Woo, 2012; Walvoord and Kurylyk, 2016; Yang and Kane, 2021). As an aquiclude, frozen ground reduces infiltration and recharge to groundwater, increases soil moisture, and enhances rainfall runoff generation (Cuo et al., 2013; Koch et al., 2024; Woo, 2012). Changes in the ground temperature gradient alter soil hydraulic conductivity and impact soil water movement as well as water storage in the active layer (*e.g.*, Gao et al., 2022; He et al., 2020; Walvoord and Kurylyk, 2016). These substantially control the subsurface hydraulic connections and alter the surface, subsurface, and groundwater flows and their discharges to rivers and lakes (Ma et al., 2021; Quinton et al., 2000; Woo and Marsh, 2005). Thus, the freeze−thaw processes fundamentally alter the magnitude and temporal patterns of runoff in permafrost terrains (*e.g.*, Gao et al., 2021; Song et al., 2021; Zheng et al., 2018) and affect the water and energy exchanges between land and atmosphere (Ma et al., 2024; Wani et al., 2021; You et al., 2017).

Runoff regimes in permafrost environments have mainly been investigated using hydrological models (*e.g.*, Bense et al., 2012; Gao et al., 2018; Wang et al., 2023) and stable or radioactive isotope tracing methods (*e.g.*, Li et al., 2024; Yang et al., 2023; Yi et al., 2018). Notably, most permafrost hydrological models on the QTP are based on the *priori* assumption that permafrost significantly impacts the runoff processes, *i.e.*, as an aquitard, the presence of permafrost and the ensued rapid runoff generation during thaw season enhances peak flows and amplifies runoff seasonal variability (Gao et al., 2021; Jin et al., 2022; Zhang et al., 2024). However, such a significant influence has not always been verified in large forested basins (Lindström et al., 2002; McClelland et al., 2004; Shanley and Chalmers, 1999) and in basins with less than 40% permafrost coverage in the Arctic (Ma et al., 2019; Ye et al., 2009). Complex physical-based models, particularly the distributed hydrology models coupled with soil freeze−thaw processes, usually require high-resolution driving data and detailed parameterization schemes, which are generally lacking or inadequately approximated in permafrost environments (Chen et al., 2018; Gao et al., 2021; Wang et al., 2017; Wang et al., 2021). This is particularly true for the cold and alpine permafrost environment with complex terrains on the QTP.

Permafrost is most common in remote areas with rare human activities at high elevations or high latitudes. Field observations, instrument maintenance, and logistical supplies are difficult and expensive tasks in permafrost environment in the HMA, due to the harsh climate and poor road accessibility. This results in very limited ground-based observational data for ungauged or poorly gauged permafrost watersheds. Furthermore, the effects of freeze−thaw processes on runoff dynamics have been heavily impacted by the land use and land cover change in the region (Woo, 2012; Woo and Marsh, 2005). However, the interactions among permafrost, ecology, and hydrology remain unknown (Wang et al., 2012a; Grünberg et al., 2020; Shur and Jorgenson, 2007), and only limited understanding of the mechanisms of permafrost hydrology has been achieved at the slope to basin scales. Thus, it is largely uncertain or evasive to simulate and predict rainfall−runoff processes for ungauged or poorly gauged permafrost watersheds using detailed distributed models (Wang et al., 2017; Loukas and Vasiliades, 2014). Permafrost hydrology studies based on the stable or radioactive isotope methods necessitate the collection of large amounts of water and soil samples in different seasons, and these methods are also based on some assumptions (Du et al., 2024; Li et al., 2020b; Xiao et al., 2020). For example, it is assumed that the isotopic composition of the water is spatiotemporally constant and any variations are caused by water mixing along the flow-paths in the end-member mixing analysis (Li et al., 2020b). There are critical knowledge gaps in process-level understanding of permafrost hydrology, due to the heterogeneity of permafrost landscapes, difficulties in data acquisition, and limited interdisciplinary research (Koch et al., 2024; Woo, 2012; Walvoord and Kurylyk, 2016). Consequently, systematic observations and studies on permafrost hydrology at the basin scale serve as the physical basis for the model simulation and prediction of permafrost hydrology, especially that in ungauged or poorly gauged watersheds in the HMA.

Please cite this article as: WANG, Q.-F et al., Water budgets in an arid and alpine permafrost basin: Observations from the High Mountain Asia, Advances in Climate Change Research, https://doi.org/10.1016/j.accre.2024.09.005

In this study, the Shuangchagou (SCG) permafrost basin, located in the Lena Qu (River) watershed in the hinterland of the headwater area of the Yellow River (HAYR) on the northeastern QTP, was selected for conducting hydrological and meteorological observations and for calculating runoff discharge. We calculated evapotranspiration based on eddy covariance (EC) observation data using the Priestley−Taylor equation, analyzed the inter-annual variations of runoff, precipitation, changes in water storage, and evapotranspiration, and discussed the impacts of freeze−thaw processes in the active layer in wetlands on runoff and runoff generation mechanisms in alpine permafrost basins. This study may contribute to and help validate hydrological model simulation and prediction, as well as provide crucial support for decision making for water resource assessment and management in the Yellow River Basin, especially in the HAYR. It also contributes to a better understanding of permafrost hydrology and runoff generation mechanisms, as well as case studies for permafrost hydrology research in ungauged or poorly gauged watersheds in the HMA.

2. Study area

The HAYR lies on the margin of the modern East Asian monsoon region (Wang et al., 2020a, 2022a), and is located in a transition zone from discontinuous to sporadic permafrost zones on the northeastern QTP (Fig. 1a). It covers an areal extent of 2.97×10^4 km^2, with several dominated landforms, such as plains, hills, low-relief mountains, and highlands (Li et al., 2016). According to records during 1953−2018, the mean annual air temperature was −3.1 °C and annual precipitation was 282 mm at the Madoi meteorological station in the northeastern HAYR, with precipitation mostly concentrated from May to September, accounting for 65%−90% of the total annual precipitation (Wang et al., 2019a, 2022b).

The HAYR is critical to the supply of water resources in the Yellow River basin. It is an important functional area of water conservation and an ecological barrier to China's ecological security (Yin et al., 2016). Permafrost is mainly distributed above 4300 m a.s.l. in fluvial plains and on the north-facing slopes and above 4500 m a.s.l. on the south-facing slopes (Li et al., 2016; Jin et al., 2009; Luo et al., 2018). In the HAYR, the areal extent of permafrost accounts for ~85% of the total area (Sheng et al., 2020, Fig. 1b), and the ground ice storage in permafrost, is preliminarily estimated at 49.6 ± 18.0 km^3 at depths of 3.0−10.0 m (Wang et al., 2017).

In the Lena Qu (River) watershed, located in the south of the Gyaring and Ngöring Lakes in the HAYR, hydrological and meteorological observations were conducted in the SCG permafrost basin (34°38′−34°40′ N; 97°18′−97°20′ E; Fig. 1a−d). This basin covers an areal extent of 15.7 km^2, with elevations ranging from 4300 to 4650 m a. s. l. The most common landform types include gentle and rolling hills, alluvial and slope-wash plains and platforms, and river valley plains. Alpine steppes and alpine wetlands dominate in land cover types (Fig. 1d), with herb coverage of mainly <40% and 40%−98%, respectively, in these two types. Alpine steppes cover elevations ranging from 4300 to 4650 m a. s. l. in the basin, while wetlands mainly occur with elevations ranging from 4300 to 4350 m a. s. l. In alpine steppes, *Stipa purpurea* Griseb. dominates, and there are several associated species, such as *Poa pratensis* Linn. and *Leontopodium nanum* Hand. The dominant species in alpine wetlands are *Kobresia humilis* (C. A. Mey ex Trauvt.) Sergievskaya, *K. capillifolia* (Decne.) C. B. Clarke, *K. humilis*, *Poa pratensis* Linn., *Littledalea racemosa*, and *Puccinellia distans* (L.) Parl. In the SCG Basin, the areal extent of alpine wetlands (including the degraded alpine wetlands) covers ~1.7 km^2, accounting for ~11% of the entire basin area, while alpine steppes cover the rest. The severely degraded alpine wetland, often covering dozens of square meters, was to intersperse the lower north branch of the stream near the basin outlet (Fig. 1d). According to field survey results in the SCG Basin, except for some partially sunny slopes of the north and south branches and the degraded alpine wetlands in the valley plains, which are possibly underlain by open or closed taliks, the rest of the basin is are mostly underlain by warm alpine permafrost (Fig. 1c). In the investigated SCG basin, turf hummocks develop extensively in the zones of alpine wetlands, and surface waters accumulate in thermokarst depressions in the thaw season from May to October.

3. Data and methods

3.1. Runoff observation and calculations

The most common method for estimating continuous streamflows is the stage−discharge relationship, known as Flow Rating Curves (FRCs) (Chow, 1959; Fenton and Keller, 2001; Kumar, 2011). The FRCs are usually calibrated to gauging stations, which are synchronized observations of water level and discharge during specific field campaigns (Manfreda et al., 2020; Rojas et al., 2020; WMO et al., 2010).

In mid-April 2014, a rectangular hydrological monitoring section was installed at the stream outlet in the SCG Basin. To prevent water leakage, the bottom of the hydrological section was set on the impervious bedrock. From late April to October, the flow velocity (V) at the hydrological section was measured using the LS10B Propeller Velocity Meter (produced by Chongqing Huazheng Hydrological Instrument Co. Ltd., China), and meanwhile, the flow depth (h) was measured using a water ruler. Then, the runoff (Q) could be calculated using the water cross-section area (Ω) at the gauging station and the flow velocity (V) according to Eq. (1). The water cross-sectional area (Ω) was calculated by multiplying the width (w) of the rectangular hydrological section by the measured flow depth (h). The LS10B Propeller Velocity Meter had a measurement range of 0.1−4.0 m s^{-1} (within a working water depth of 1.2 m), a mean square deviation of the verification formula ≤1.5%, and an operating environment temperature range of −10 to 45 °C.

Please cite this article as: WANG, Q.-F et al., Water budgets in an arid and alpine permafrost basin: Observations from the High Mountain Asia, Advances in Climate Change Research, https://doi.org/10.1016/j.accre.2024.09.005

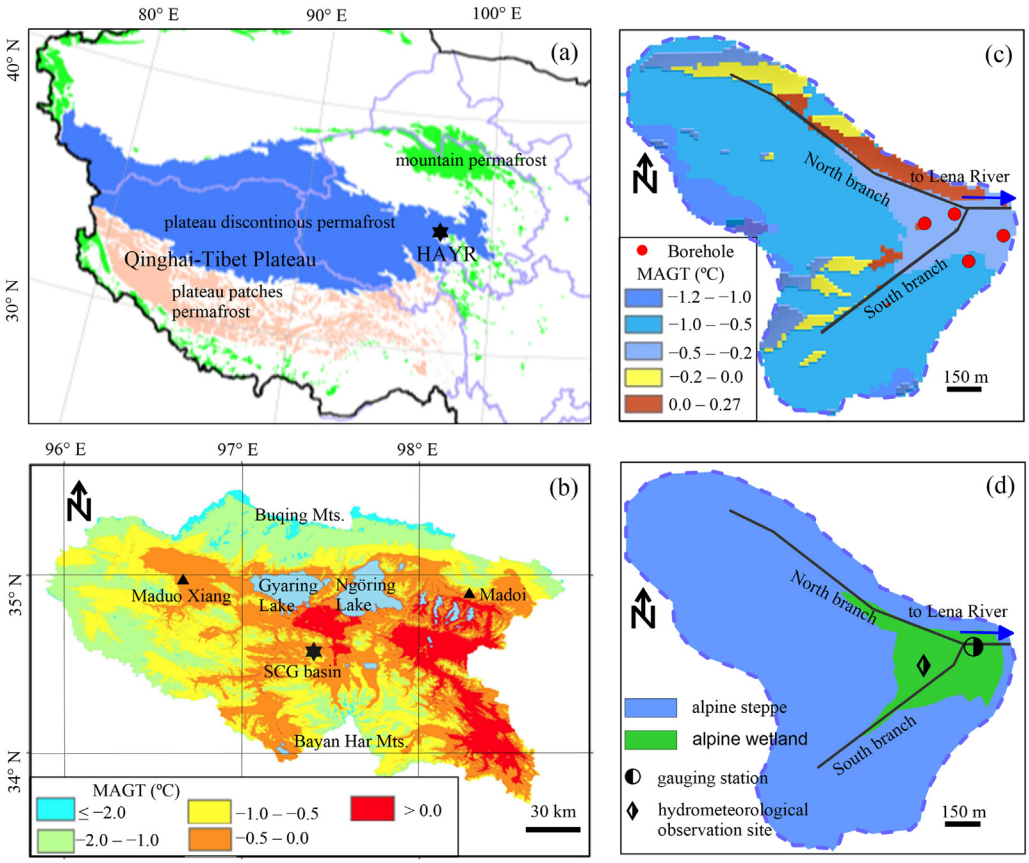

Fig. 1. The permafrost distribution on the QTP (Wang et al., 2012b) showing the location of the HAYR (a), the distribution of the mean annual ground temperature (MAGT) at depths of 10−25 m in the HAYR (b; Li et al., 2016; Sheng et al., 2020) and at a depth of 10 m in the Shuangchagou (SCG) permafrost basin (c), as well as a description of the considered hydrometric sites in the SCG basin (d).

$$Q = V \times \Omega \quad (1)$$

Then, the FRC was calculated based on the water level (h) and runoff (Q) at the gauging station following the most adopted equation (Lambie, 1978; Mosley and McKerchar, 1993; Clarke, 1999):

$$Q(t) = a \times h(t)^b \quad (2)$$

where $Q(t)$ denotes the runoff at the gauging station at time t; $h(t)$ denotes the water depth at time t, and; a and b are constants. The FRC at the gauging station in the SCG basin is shown in Fig. 2a ($R^2 = 0.91$, $p < 0.05$).

Meanwhile, the HOBO water level meter (U20-001-01) produced by the Onset Computer Corporation, USA was used to automatically measure the flow depth at the gauging station, and the water level was converted into discharge using Eq. (2) (Fig. 2a). The measurement range of the HOBO water level meter was less than 9.0 m, with an accuracy of 0.5 cm and a resolution of 0.21 cm. The automatic measurement period of the water level at the gauging station was from 20 April 2014 to 31 December 2016, with observation data missing from 13 June 2015 to 28 August 2015 and from 24 November 2016 to 31 December 2016 due to instrument battery failure.

3.2. Investigation of hydrometeorology and soil properties

A hydrometeorological station (97°19′39.6′ E; 34°38′53.4′ N, 4410 m a.s.l.) was established in the SCG permafrost basin to observe precipitation and soil hydrothermal processes in the active layer of alpine wetland (Fig. 1d). Air temperature, relative humidity and the four-component radiation flux were also measured using EC method. The instrumental site, with herb coverage of ~90%, was on the middle slope (6%) of an alluvial fan. The observation period lasted from 25 May 2014 to 24 September 2015, with a recording interval of 30 min. Precipitation was measured using a tipping bucket rain gauge, with an accuracy of ±1%. Soil temperature and volumetric water content (VWC) of the active layer were measured, with an accuracy of ±0.2 °C and ±2%, respectively (Fig. 3a) (Wang et al., 2019a). An air temperature and relative humidity sensor (HMP-45C) was used to correct flux measurements for density effects due to heat and water vapor transfers. Radiation flux was monitored using a four-component net radiometer (CNR-1). Soil heat fluxes were also measured at the investigated alpine wetland site (Table 1).

Please cite this article as: WANG, Q.-F et al., Water budgets in an arid and alpine permafrost basin: Observations from the High Mountain Asia, Advances in Climate Change Research, https://doi.org/10.1016/j.accre.2024.09.005

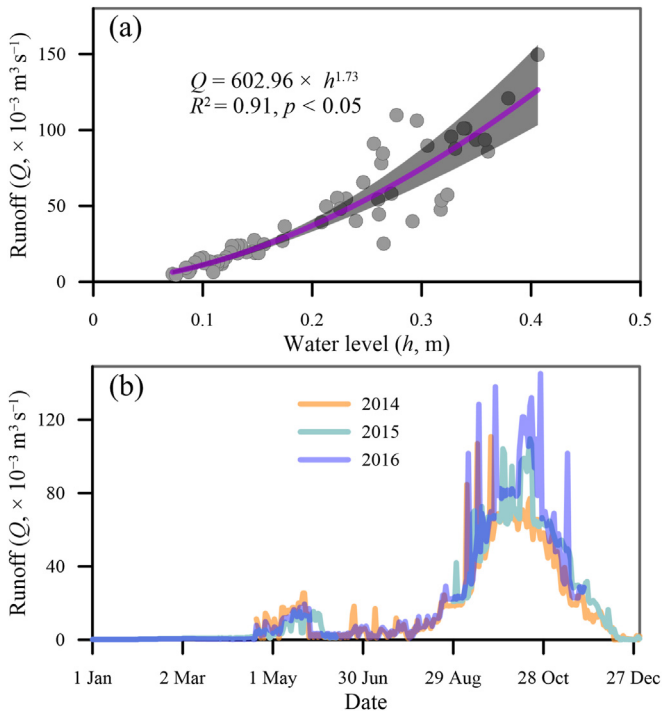

Fig. 2. Stage−discharge relationship for the gauging station (a, late April to October 2014) and hydrograph (b, June 2014 to December 2016) in the SCG permafrost basin in the HAYR on the northeastern QTP (In (a), the purple line is the best fit Flow Rating Curve (FRC), and the gray region indicates the 95% confidence interval).

A 100 cm^3 cut ring was used to collect soil samples at depths of 0−20, 20−40, 40−60, and 60−80 cm. Bulk density and saturated hydraulic conductivity (SHC) were measured using the oven-drying method and constant head method, respectively.

3.3. Water balance equation and water storage

The water balance equation at the basin scale for a given period is expressed as follows (Wang et al., 2020b):

$$P - Q - E = \Delta S \tag{3}$$

where P, Q, E, and ΔS represent precipitation, runoff flowing out of the basin, actual evapotranspiration, and changes in water storage during the study period, respectively. The changes in water storage in the basin include the changes in soil water storage (ΔS_{soil}) and those in water storage in ground surface waters in the thermokarst depressions and in groundwater (ΔS_{gg}).

Evapotranspiration is calculated based on EC observation data after data processing and gap filling (Wang et al., 2019a), using the Priestley−Taylor equation as follows:

$$E = \alpha_e \frac{\Delta}{\Delta + \gamma} Q_{ne} \tag{4}$$

$$Q_{ne} = \frac{(R_n - G)}{\rho \lambda} \tag{5}$$

where α_e is the Prestley−Taylor parameter (Priestley and Taylor, 1972); Δ is the slope of the saturation vapor pressure curve relative to the temperature (kPa °C^{-1}); γ is the slope psychrometric constant (kPa °C^{-1}); Q_{ne} is the available energy expressed in evaporation units (mm); R_n is the net radiation (W m^{-2}); G is the soil heat flux (W m^{-2}) at a depth of 5 cm; ρ is the density of liquid water (kg m^{-3}) and λ is the latent heat of water vaporization (kJ kg^{-1}).

Water storage in a soil column with the unit ground-surface area S_{soil} (unit: mm) can be evaluated by summing the water storage in each sub-layer:

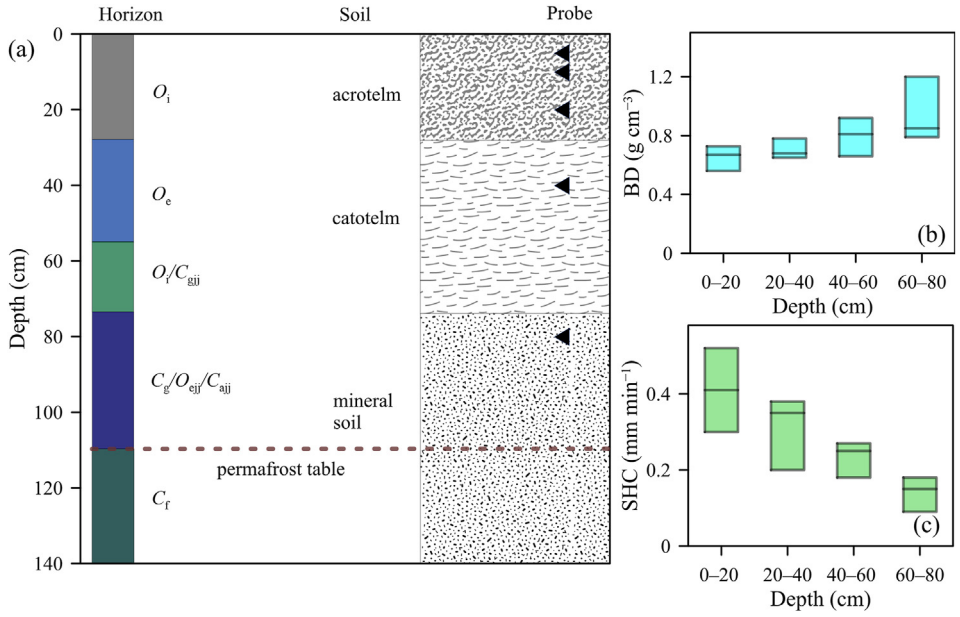

Fig. 3. Soil horizons, distribution of organic and mineral layers, and the placement depths of soil temperature and moisture probes (black triangles; a), bulk density (b), and saturated hydraulic conductivity (SHC) (c) in the investigated alpine wetland soil profile.

Please cite this article as: WANG, Q.-F et al., Water budgets in an arid and alpine permafrost basin: Observations from the High Mountain Asia, Advances in Climate Change Research, https://doi.org/10.1016/j.accre.2024.09.005

Table 1
Observation parameters and depths (or heights) of instruments in the investigated alpine wetland in the SCG permafrost basin.

Parameter	Instrument	Depth/Height (cm)
Precipitation	Tipping bucket rain gauge TE525 (Campbell Scientific Inc., USA)	Ground surface
Soil temperature	109 Temperature Probe (Campbell Scientific Inc., USA)	−5, −10, −20, −40, and −80
VWC	CS616 Soil Moisture Probe (Campbell Scientific Inc., USA)	−5, −10, −20, −40, and −80
Air temperature and relative humidity	HMP-45C sensor (Vaisala, Helsinki, Finland)	200
Radiation flux	Radiometer CNR-1 (Kipp and Zonen, Delft, Netherlands)	150
Soil heat flux	Heat plates HFT-3 (Campbell, USA)	−5 and −40

$$S_{\text{soil}} = \frac{\sum_{i}^{n}\left(\theta_{\text{u}}^{i} + \theta_{\text{l}}^{i}\right)d_i}{2} \quad (6)$$

where θ_{u}^{i} and θ_{l}^{i} are soil VWC at the upper and lower boundaries of the ith sub-layer, respectively (Yamanakaa et al., 2007); d_i (unit: mm) is the thickness of the layer; and n is the number of sub-layers. As the top layer θ_{u}^{1} cannot be measured by the CS 616 probe, we assumed $\theta_{\text{u}}^{1} = \theta_{\text{l}}^{1}$. Then, the changes in soil water storage (ΔS_{soil}) during a given period can be calculated.

4. Results

4.1. Profiled soil properties of alpine wetlands

A soil pit was excavated for soil profile description and sampling. The morphological properties of the soil were described according to Schoeneberger et al. (2021). At the investigated alpine wetland site, the soil keyed out as Ruptic Histoturbel according to the USDA Soil Taxonomy (SSS, 2014), and the active layer was 110 cm thick. The investigated alpine wetland profile consisted of cryoturbated O_{i} and O_{e} horizons at depths of 0−55 cm, an $O_{\text{e}}/C_{\text{gjj}}$ horizon at depths of 55−73 cm, a $C_{\text{g}}/O_{\text{ejj}}/O_{\text{ajj}}$ horizon at depths of 73−110 cm, and a C_{f} horizon at depths of 110−140 cm (O indicates organic soil materials; Table 1 and Fig. 3a). In the investigated profile, the broken organic horizon contained an acrotelm layer at depths of 0−28 cm and a catotelm layer at depths of 28−73 cm, and the profile was mineral soil at depths of 73−140 cm (Table 1 and Fig. 3a). At depths of 0−80 cm, bulk density increased gradually while SHC decreased, with values of 0.65−0.95 g cm^{-3} and 0.14−0.41 mm min^{-1}, respectively (Fig. 3b and c).

4.2. Variations in soil hydrothermal regimes

The ground surface in the active layer generally began to freeze in mid-to late October and to thaw in mid-to late April in the investigated alpine wetland. From mid-to late April to the next March, the variations in shallow soil temperature in the active layer took a shape of the sine function curve. With increasing depth, soil temperature fluctuation curves exponentially dwindled, and the peak values of soil temperature at a depth of 5 cm declined and delayed from 11.5 °C in mid-to late July to −0.05 °C at a depth of 80 cm in mid-September (Fig. 4a and 5b). In contrast, the lowest values of soil temperature at these two corresponding depths increased from −9.9 to −3.6 °C, and the dates of reaching the minima was delayed from early January to mid-March.

Based on the changes in the active layer soil temperature, the ground freeze−thaw processes can be divided into four stages, *i.e.*, thawing, thawed, re-freezing, and freeze-up periods (Chen et al., 2018; Pan et al., 2022). As the active layer thawed from top down, VWC increased quickly at first and then maintained at a high level. VWC decreased rapidly at the initial stage of the ground re-freezing period, while during the subsequent freeze-up period, soil unfrozen water content in the active layer remained almost stable at a low level of <10% (Fig. 4b and 5b). From mid-September to mid-October in 2014, VWC in the thawed layer at the depths of 40, 10, 20, 80, and 5 cm decreased successively, with values of 78%, 71%, 62%, 55%, and 43%, respectively.

4.3. Variations in precipitation, runoff, evapotranspiration, and ΔS

4.3.1. Precipitation

From June 2014 to May 2015, there were 265 d with precipitation (rainy or snowy days), with an average daily precipitation at 1.5 mm d^{-1}. Among them, there were only 6 d with moderate rain (10−25 mm d^{-1}), and the total precipitation in these six rainy days accounted for 19% of the annual total. The other 259 d showed light rain (<10 mm d^{-1}) with the total precipitation of 332 mm. Daily precipitation was higher from May to September, ranging from 1.1 to 3.6 mm, while it was much lower in the other months, with values ranging from 0.1 to 0.7 mm (Fig. 6a). The annual precipitation totaled 408 mm (uncorrected for dynamic and other losses) from June 2014 to May 2015, and the precipitation was mainly concentrated from May to September, accounting for 84.4% of the annual total.

4.3.2. Runoff

From January to mid-April, runoff was stable at a low level, and the daily average runoff from 2014 to 2016 ranged from 0.2×10^{-3} to 1.0×10^{-3} m^3 s^{-1} (Fig. 2a and b). The streamflow increased greatly from mid-April to late May, resulting in a spring flush flood, with daily runoff ranging from 1.0×10^{-3} to 17.4×10^{-3} m^3 s^{-1}; and afterwards, the daily runoff remained relatively stable until late June, with values ranging from 1.2×10^{-3} to 6.7×10^{-3} m^3 s^{-1}. The runoff gradually increased from late June to late October, and showed

Please cite this article as: WANG, Q.-F et al., Water budgets in an arid and alpine permafrost basin: Observations from the High Mountain Asia, Advances in Climate Change Research, https://doi.org/10.1016/j.accre.2024.09.005

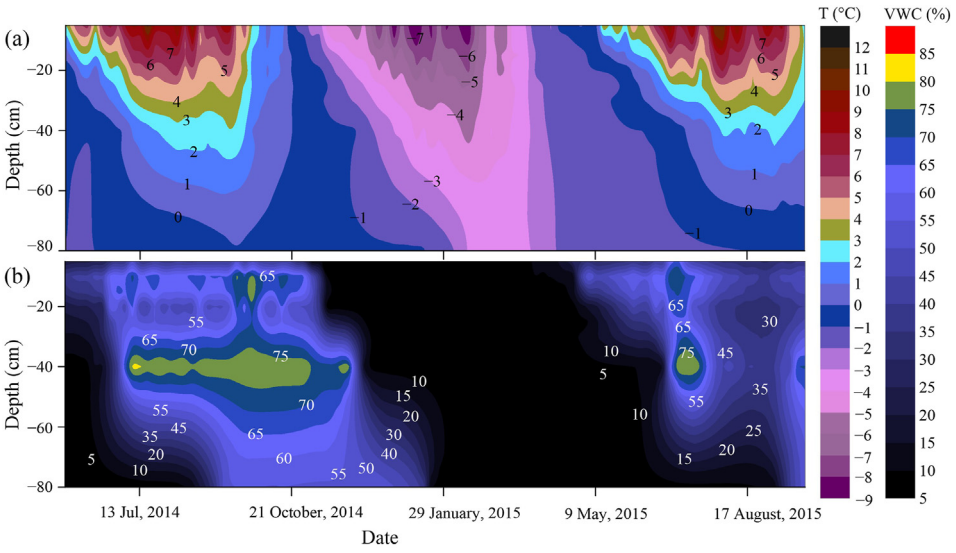

Fig. 4. Contour maps of soil temperature (a) and volumetric moisture content (VWC) (b) in the active layer freeze−thaw processes of the investigated alpine wetland in the SCG permafrost basin in the HAYR from 25 May 2014 to 24 September 2015.

a significant autumn flood from mid-September to late October, with daily runoff ranging from 44.0 × 10^{-3} to 133.0 × 10^{-3} m^3 s^{-1}. Then, the daily runoff gradually decreased to ~0.2 × 10^{-3} m^3 s^{-1} in mid-to late January (Fig. 2a and b). Although daily runoff during the spring flood season accounted for only ~11% of that during the autumn flood season, it was 5−17 times that of daily runoff in days around the spring flood season.

The daily runoff depth was higher from September to November, ranging from 0.15 to 0.43 mm, followed by that in May and August with values of 0.05−0.06 mm, and; it was prominently lower in other months, with values of ≤0.03 mm (Fig. 6b). Monthly runoff depth decreased from 2.0 mm in May to 0.5 mm in June, and it gradually increased to 10.8 mm in October. It decreased from 4.5 mm in November to 0.002 mm in January 2015, with values ranging of 0.05−1.5 mm from February to May. Data were missing from June to August 2015, and monthly runoff depth ranged from 6.6 to 13.2 mm from September to November, with a value of 0.9 mm in December (Fig. 6d).

4.3.3. Evapotranspiration and ΔS

The daily evapotranspiration was between 1.5 and 3.2 mm from June to October 2014, with values of 0.2−1.9 mm d^{-1} from December 2014 to April 2015, and between 1.7 and 3.6 mm from May to September 2015 (Fig. 5d). The monthly evapotranspiration ranged from 47.7 to 100.1 mm from June to October 2014, with values of 7.0−58.0 mm from December 2014 to April 2015. The monthly evapotranspiration ranged from 49.6 to 107.2 mm from May to September 2015 (Fig. 6e).

From June 2014 to September 2015, the monthly ΔS was positive in June, August and September 2014 and September 2015, with values of 3.0−41.1 mm; while it was all negative in other months, with values ranging from −4.2 to −49.9 mm (Fig. 6d). That is to say, except an enhanced water storage in

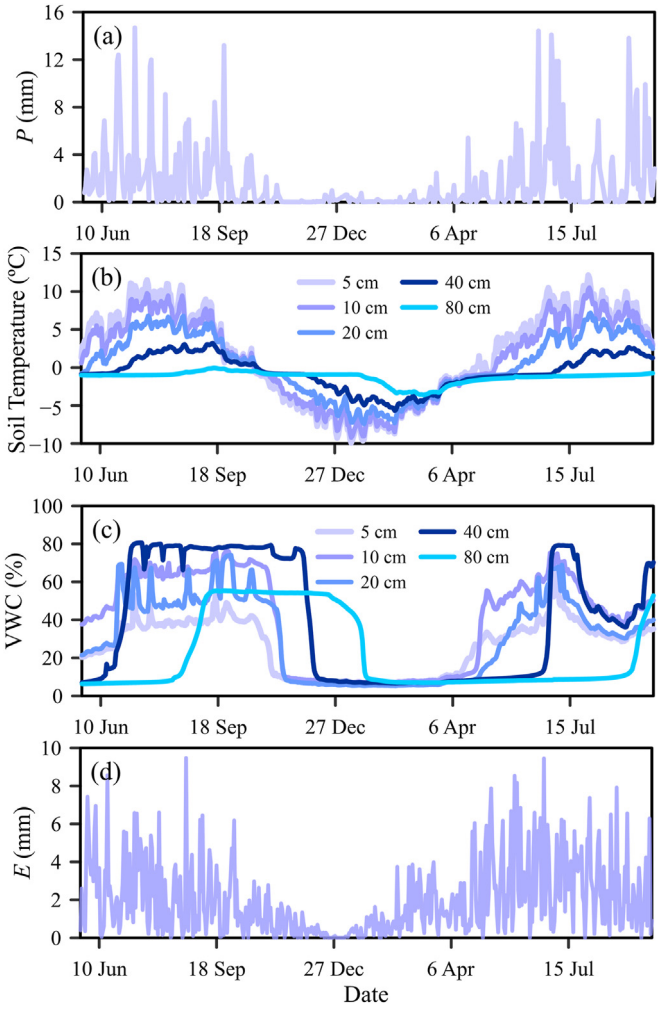

Fig. 5. Daily precipitation (a), active layer soil temperature (b), soil volumetric moisture content (c) and evapotranspiration (d) in the investigated alpine wetland site in the SCG permafrost basin in the HAYR from 25 May 2014 to 24 September 2015.

Please cite this article as: WANG, Q.-F et al., Water budgets in an arid and alpine permafrost basin: Observations from the High Mountain Asia, Advances in Climate Change Research, https://doi.org/10.1016/j.accre.2024.09.005

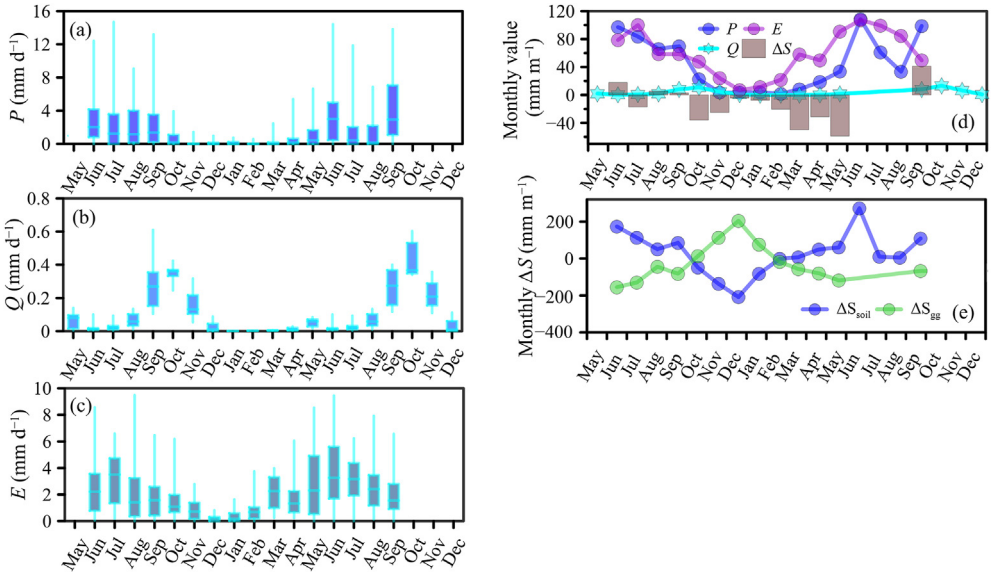

Fig. 6. Variations of daily precipitation (a), runoff depth (b), and evapotranspiration (c), monthly *P*, *Q*, *E*, and Δ*S* (d), as well as monthly changes in soil water storage (ΔS_{soil}) and those in water storage in ground surface waters in the thermokarst depressions and in groundwater (ΔS_{gg}) (e) in the SCG permafrost basin from May 2014 to December 2015.

the alpine wetland ecosystem in June, August and September, it was all deficient in other months during the investigated period. The monthly ΔS_{soil} was deficient from October to February due to decreases in unfrozen water content caused by the ground freeze process in the active layer and the decreasing air temperature, while it was all positive in other months during the investigated period (Fig. 6e).

5. Discussion

5.1. Evapotranspiration variations in alpine wetlands

The accurate estimate of evapotranspiration in terrestrial ecosystems is essential for better understanding regional to global water budgets and hydrological cycle. At the investigated alpine wetland site, daily evapotranspiration averaged 2.4 mm d^{-1} in 2014 and 2.8 mm d^{-1} in 2015 in the growing season, and it averaged 0.95 mm d^{-1} in the non-growing season (Fig. 6d). Daily average evapotranspiration was 1.5−2.9 mm d^{-1} in the seasonal transition period (*i.e.*, October and May; Fig. 6d). The annual evapotranspiration and evapotranspiration in the growing and non-growing seasons at the investigated wetland site were 607, 435 and 172 mm, respectively. These results were similar to those found at the Arou station in eastern Qilian Mountains (Tong et al., 2018). Yet, they were prominently lower than those found at the Haibei station in the eastern Qilian Mountains (Zhang et al., 2018) and in the Fenghuoshan Mountains on the interior QTP (Xiao et al., 2023; Zhang et al., 2023a), based on several methods, such as Priestley−Taylor equation, Penman−Monteith equation, Weighing lysimeters, and EC method (Table 2). Much lower evapotranspiration in the growing season were observed, ranging between 247 and 321 mm, at the alpine meadow site in the Tanggula Mountains on the interior QTP (Table 2; Wang et al., 2019b). These were probably caused by differences in precipitation, net radiation, air and ground-surface temperatures, ground surface soil moisture contents, and leaf area index among these sites. Additionally, the main influencing factors for evapotranspiration in the growing and non-growing seasons of alpine meadows may differ. Evapotranspiration in the growing season is mainly influenced by net radiation and air/ground-surface temperature, whereas soil moisture availability/content and net radiation are dominated influencing factors for evapotranspiration in the non-growing season (Zhang et al., 2018; Dai et al., 2021).

The ratio of annual evapotranspiration to precipitation was 1.5 at the investigated alpine wetland site, and similar values were also found at the Arou station (Tong et al., 2018), in the Tanggula Mountains (Wang et al., 2019b), at the Haibei station (Zhang et al., 2018), and in the Fenghuoshan Mountains (Table 2) (Xiao et al., 2023; Zhang et al., 2023a). This is mainly due to the considerably underestimated 'observed' precipitation, which is also proved by the high runoff coefficients and accumulated snow water equivalent exceeding contemporaneous precipitation in the HMA (Miao et al., 2024). In the HMA, ~40% of the precipitation occurs in the form of snow as indicated by satellite radar observations (Song and Liu, 2021), and precipitation is typically accompanied by strong winds. The limited cross-sectional area in the precipitation collection cylinder and the sealed bottom in traditional rain gauges cause an upward supporting airflow to arise under windy circumstances (Miao et al., 2024). This hinders raindrops or snowflakes from entering the precipitation gauge cylinder, thereby resulting in an underestimation of precipitation in this region. This wind-induced instrumental error constitutes the largest bias affecting precipitation measurements at high-altitudes (Ye et al., 2004). Thus, it is crucial to enhance precipitation

Please cite this article as: WANG, Q.-F et al., Water budgets in an arid and alpine permafrost basin: Observations from the High Mountain Asia, Advances in Climate Change Research, https://doi.org/10.1016/j.accre.2024.09.005

Table 2
Comparisons of evapotranspiration at the investigated alpine wetland site in the SCG permafrost basin in the HAYR with the published results of alpine weadows in the other regions on the QTP.

Location	Elevation (m)	MAAT (°C)	P_{ann} (mm)	Study period	Method	E_{ann} (mm)	E_{ann}/P_{ann}	Reference
Arou station in the Qilian Mts.	3044	−0.4	520	2014	Two-source model	520;[a] 408;[bd] 112;[c]	1.0	Tong et al. (2018)
	3044	−0.3	401	2015	Two-source model	551;[a] 422;[bd] 129;[c]	1.4	Tong et al. (2018)
Tanggula Mts.	5170	−5.0	437	2007−2013	Weighing lysimeters	247−321[be]	/	Wang et al. (2019b)
Haibei station in the Qilian Mts.	3200	−1.7	684	2018−2019	Simplifed Priestley−Taylor equation	1050;[a] 768;[be]283;[c]	1.5	Zhang et al., 2018
		−1.7	684	2018−2019	Penman−Monteith equation	937;[a] 805;[be]132;[c]	1.4	Zhang et al., 2018
		−1.7	684	2018−2019	Weighing lysimeters	1189;[a] 802;[be]387;[c]	1.7	Zhang et al., 2018
Fenghuoshan Mts.	4809	−4.7	386	2019	EC method	475[bf]	>1.2	Zhang et al., 2023
		−4.7	386	2019	Penman−Monteith equation	518[bf]	>1.3	Zhang et al., 2023
		−4.7	386	2019	Weighing lysimeters	493[bf]	>1.3	Zhang et al., 2023
Fenghuoshan Mts.	4809	−4.7	385	2019−2020	Weighing lysimeters	479[bg]	>1.2	Xiao et al. (2023)
SCG basin in the HAYR	4410	−2.9	412	2014−2015	Priestley−Taylor equation	607;[a] 435;[be] 172;[c]	1.5	This study

Notes: MAAT, P_{ann}, and E_{ann} indicate mean annual air temperature, annual precipitation, and annual evapotranspiration, respectively. [a] annual; [b] growing season; [c] non-growing season; [d] indicates from May to September; [e] June to September; [f] 11 April to 10 October; and [g] 20 April to 17 October.

monitoring through the development of instruments that can resist external interference such as wind and are proficient in measuring solid precipitation (Miao et al., 2024). Additionally, snow sublimation plays an important role in the Arctic moisture budget (Liston and Sturm, 2004). Nevertheless, compared with Arctic, snow depth is limited in the study area. The mean annual snow depth from 1979 to 2020 in the Yellow River Basin on the northeastern QTP was 1.0 mm (Liu et al., 2024), and the influence of snow sublimation was not considered in this study. The high ratio of annual evapotranspiration to precipitation also partly indicates that, besides precipitation, soil water storage and ground ice in the active layer of the wetland also provide water source for water consumption. Topsoil has a strong soil water holding capacity due to the mattic epipedons in the growing season of alpine wetlands (Zhang et al., 2023b; Yang et al., 2014). Soil water (*i.e.*, unfrozen water in frozen soils), distillation and convection of water vapor, and ground ice in the active layer of alpine wetlands could also provide water source for evapotranspiration during the non-growing season (Hinkel et al., 2001). From January to May, in July, and from October to December, the deficient ΔS in the investigated wetland ecosystem was due to that evapotranspiration needs to consume a large amount of ground-surface liquid waters, soil water, and/or ground ice in the active layer (Hinkel et al., 2001). In short, the high ratio of annual evapotranspiration to precipitation in investigated alpine permafrost wetland was due to the considerably underestimated 'observed' precipitation, the influence of snow sublimation, and the fact that wetlands serve as water source providers rather than consumers.

5.2. Variations in soil VWC in the freeze−thaw processes of the active layer in alpine wetlands

During the thawing and thawed periods in the active layer of alpine wetlands and tundra, variations in VWC in the thawed layers were mainly due to infiltration of rainfall or meltwater (Hinkel et al., 2001; Zhao et al., 2000; Lopez et al., 2010), downslope subsurface drainage from higher elevations that occurred predominantly in organic soils (Woo and Marsh, 2005; Quinton et al., 2000, 2003), thawing of ground ice or snow/ice covers (Hinkel et al., 2001), and evapotranspiration (Zhang et al., 2018). In hummocky permafrost tundra, high hydraulic conductivity caused preferential flow in the acrotelm layer and subsurface slow flow in the catotelm layer (Woo and Marsh, 2005; Quinton and Marsh, 1998; Quinton et al., 2000). Subsurface water flow discharge, which occurred mainly within the peat layer and could be as rapid as the ground surface flow, was the predominant mechanism of water migration on the permafrost-affected slopes in tundra (Quinton et al., 2000). Considering that soil pores were seldom fully ice-filled, infiltration into the frozen organic soils was found to be usually unimpeded (Woo and Marsh, 2005). Evapotranspiration mainly influences the variations in VWC in shallow soil layers. Thus, in addition to the infiltration of rainfall or meltwater in the ground thaw process of the active layer, subsurface lateral flow is discharged downslope predominantly through a tortuous network in alpine wetlands.

From mid-September to mid-October, soils at depths of 5−80 cm in the active layer were thawed, and there was a

Please cite this article as: WANG, Q.-F et al., Water budgets in an arid and alpine permafrost basin: Observations from the High Mountain Asia, Advances in Climate Change Research, https://doi.org/10.1016/j.accre.2024.09.005

progressive decline in soil VWC at depths of 40, 10, 20, 80, and 5 cm. On the one hand, the plant roots of alpine meadows on the QTP are mainly distributed in the mattic epipedon (O_i horizon) at depths of 0−20 cm (Zhang et al., 2023b; Yang et al., 2014), resulting in higher VWC at depths of 10 and 20 cm. Alternatively, the interactions among rainfall or meltwater infiltration on the replenishment of soil VWC in shallow layers, soil water retention, and evapotranspiration resulted in lower VWC at a depth of 5 cm than that at depths of 10−80 cm, with lower VWC at depths of 10 and 20 cm than that at the depth of 40 cm. The soil layer at depths of 0−20 cm in the O_i horizon of the investigated alpine wetland profile is also known as the mattic horizon in the Chinese Soil Taxonomy (Yang et al., 2014; Zeng et al., 2013; Ruehlmann and Köschens, 2009), which is characterized by dense grassroots, high organic matter content, low bulk density, and soil crumb structure. Roots at depths of 0−20 cm accounted for more than 80% of root biomass in alpine meadows on the QTP, and root density declined rapidly with depths (Yue et al., 2015; Zhou et al., 2005). The dense root network and soil crumb structure in the mattic horizon can significantly boost infiltration and storage of rainfall or meltwater in meadows. Bulk density increased gradually with depth between 0 and 80 cm in the active layer, and it increased by 46% at depths of 60−80 cm compared with that at depths of 0−20 cm (Fig. 3b). Bulk density, being largely a function of soil organic matter content, has close correlations with soil porosity and water retention ability (Ruehlmann and Köschens, 2009). The high organic matter content in the mattic horizon was found to play a dominant role in controlling soil water retention in the alpine cold environment on the northeastern QTP (Yang et al., 2014).

The freeze process of the active layer includes the re-freezing (*i.e.*, two-way freezing) stage and the freeze-up stage (Pan et al., 2022). As the freezing temperature of soils decreased in the ground freeze process, unfrozen water content (θ) declines nonlinearly along with the absolute value of soil temperature ($|T|$), following a power function ($\theta = c \times |T|^d$); c and d are the fitting parameters) with median $c = 18.17$ and $d = -0.75$ (Fig. 7a−e). During the re-freezing stage, soil water in the unfrozen layer between the two freezing fronts migrates to the frozen fronts in the form of capillary water and water vapor (Hinkel et al., 2001), and it mainly migrates downwards (Zhao et al., 2000). During the subsequent freeze-up stage, unfrozen water migrates upwards, but the amount of water migration is much less than that in the re-freezing stage (Zhao et al., 2000).

5.3. Possible mechanisms for slope runoff in the arid and alpine permafrost basin

From early May to late October, the mechanisms for slope runoff in the alpine permafrost wetlands, with well-developed organic horizon and ice-rich mineral horizon, belong to the 'fill−and−spill' runoff generation mode (Wang et al., 2020b; Spence and Woo, 2003). Precipitation is converted into runoff after vegetation interception and supplementing the water deficiency in the vadose zone in the alpine permafrost wetlands *via* surface, subsurface, and groundwater (supra-permafrost water) flows. While vertical percolation dominates and negligible runoff occurs in alpine steppes and desert steppes at higher elevations in the investigated SCG permafrost basin, with no organic soil and ice-poor mineral soils in the active layer (Fig. 8).

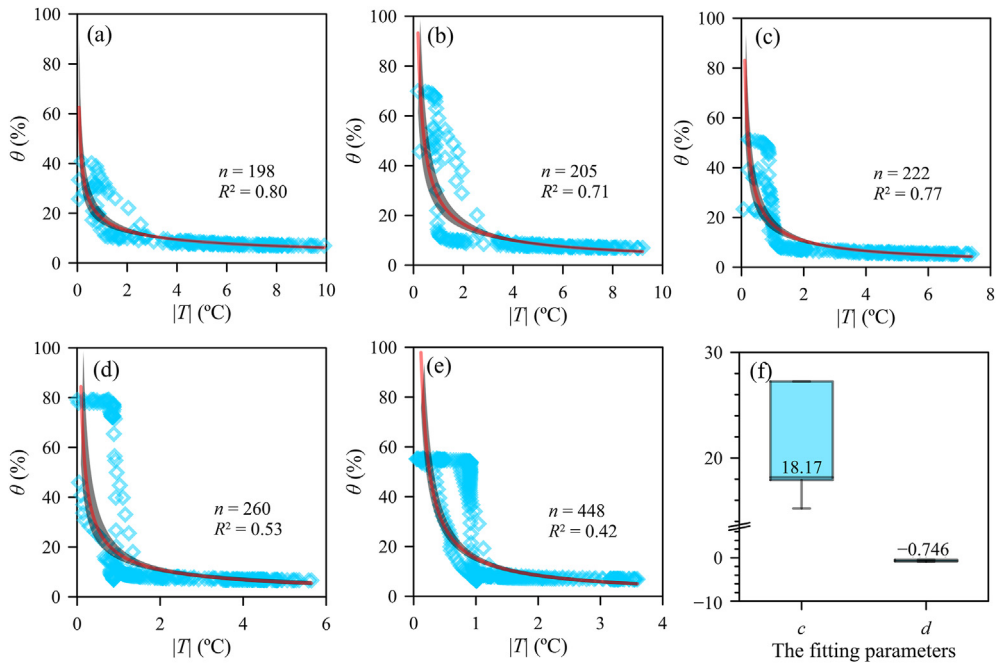

Fig. 7. Relationship between unfrozen water content (θ) and soil temperature (T) at depths of 5 cm (a), 10 cm (b), 20 cm (c), 40 cm (d), and 80 cm (e) in the SCG permafrost basin in the HAYR during the ground freezing and frozen process in the active layer of the investigated alpine wetland from May 25, 2014 to September 24, 2015, and the fitting parameters ($\theta = c \times |T|^d$) (f) (The solid curves and shadowy regions denote the fitting curves and the 95% confidence intervals, respectively).

Please cite this article as: WANG, Q.-F et al., Water budgets in an arid and alpine permafrost basin: Observations from the High Mountain Asia, Advances in Climate Change Research, https://doi.org/10.1016/j.accre.2024.09.005

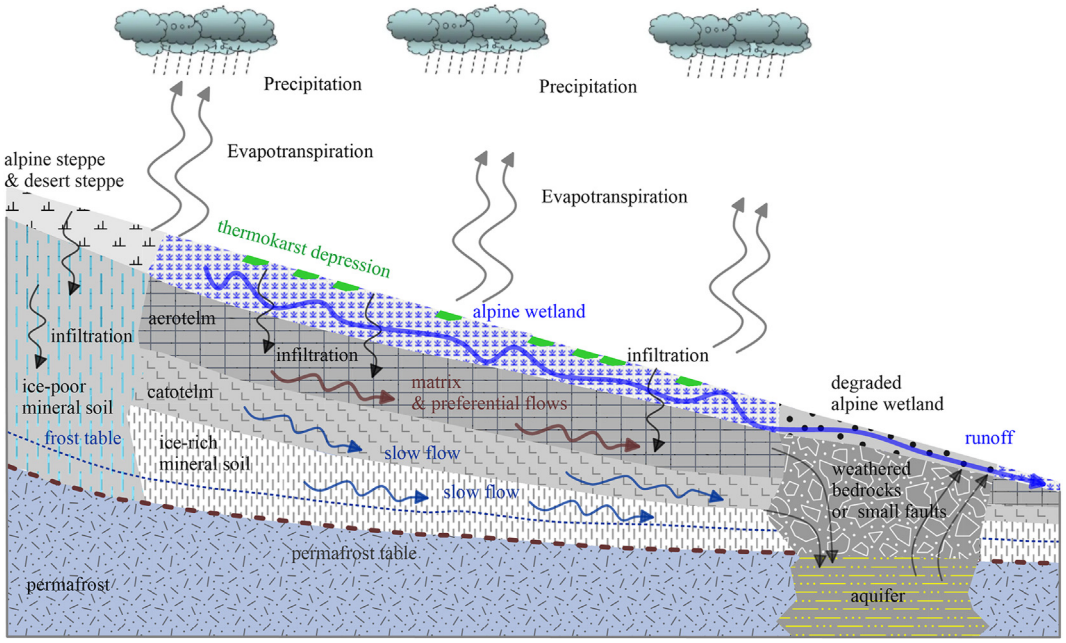

Fig. 8. The probable diagram of the mechanisms for slope runoff in the SCG permafrost basin in the HAYR on northeastern QTP, during the ground thaw process of the active layer (modified from Woo and Marsh (2005)) from May to late October.

During the field investigations, it has been found that surface runoff is only generated under certain rainfall conditions in alpine wetlands close to the stream in the SCG permafrost basin from May to October; and no surface runoff occurs in the other alpine wetlands during this period. Obviously, the continuous runoff in the stream from May to October can possibly come from the lateral discharge of subsurface flow in the alpine permafrost wetlands. When the infiltration capacity of the lower layer is significantly lower than that of the upper layer in soils with layered structures, the infiltration water flow will be hindered and accumulated at the interface, forming a saturation zone and a lateral hydraulic gradient. As a result, subsurface flow occurs, including matrix flow and preferential flow (*i.e.*, a non-equilibrium pipe flow conducted through soil macropores) (Quinton and Marsh, 1998; Woo and Marsh, 2005). The organic layer in the investigated alpine wetland contained an acrotelm layer at depths of 0−28 cm and a catotelm layer at depths of 28−73 cm (Fig. 3a). The acrotelm is hydrologically active, whereas the cartotelm is humified and compacted (Quinton and Marsh, 1998; Woo and Marsh, 2005). The SHC decreased by 66% within depths of 0−80 cm in the investigated alpine wetland (Fig. 3c). In hummocky permafrost terrains in Arctic tundra, the hydraulic conductivity of Histels decreased by two to three orders of magnitude within a depth of 30 cm below the ground surface (Quinton et al., 2000), and the hydraulic conductivity of peat soils was two to six orders of magnitude higher than that of mineral soils (Quinton et al., 2000). The SHC decreased by more than 90% at depths of 0−60 cm of the mat-cryic Histels in the permafrost wetlands in the Qilian Mountains (Xiao et al., 2020). Preferential flow mainly occurs in the acrotelm whereas slow flow occurs in the catotelm and mineral soils (Woo and Marsh, 2005).

Due to the continuous flow at the watershed outlet in winter (Fig. 2a), it is indicated that the deep aquifer discharges from weathered bedrocks or probably some small faults beneath the ‘exposed black soil spots’ along the lower part of north branch of the stream. From late May through October, the deep aquifer may also receive discharge from subsurface flow, runoff, precipitation infiltration, and supra-permafrost water in alpine wetlands (Fig. 8). Upward groundwater flow from aquifer of the taliks might also replenish the runoff in autumn in the discontinuous permafrost zone. Nevertheless, alterations in hydraulic heads and hydraulic gradients in the aquifer of the taliks in the SCG permafrost basin are not investigated in this study. In addition, the scale of hydrology may also lead to a certain degree of uncertainty in runoff, that is, the runoff of the small catchment, especially the subsurface flow, may also come from the surrounding area of the catchment.

When the soil VWC of the active layer is close to saturation in the vadose zone of the wetlands, surface flow may occur in the low relief through the marsh−depression−channel pathways flowing to the basin outlets (Quinton et al., 2003). As indicated by the two-component mixing model of δ^2H values in the stream, the average contribution of new water (*i.e.*, precipitation) and old water (*i.e.*, soil water and supra-permafrost water) to the stream from mid-July to late August was 2% and 98%, respectively, on the permafrost hillslope of alpine wetland in the Binggou Basin in the Qilian Mountains (Xiao et al., 2020). Additionally, old water mainly originated from shallow subsurface flow at depths of 30−60 cm in alpine wetlands (Xiao et al., 2020). Deterministic hydrological models revealed that, the contributions of surface, subsurface, and supra-permafrost water flows to runoff in alpine wetlands from summer to autumn in the Binggou Basin, were 7%, 65%, and 28%, respectively (Yang et al., 1992). Lateral

Please cite this article as: WANG, Q.-F et al., Water budgets in an arid and alpine permafrost basin: Observations from the High Mountain Asia, Advances in Climate Change Research, https://doi.org/10.1016/j.accre.2024.09.005

subsurface flow dominated runoff during rainfall periods in tundra and subarctic permafrost environments, with most of flow passing through the organic layer, whereas negligible runoff was generated on slopes without organic soils in the active layer in the Wolf Creek Basin, Yukon (Woo and Marsh, 2005). Similarly, subsurface flow was important in runoff in cold alpine basins (Li et al., 2014, 2019) and forested catchments (Lischeid, 2008; McGuire and McDonnell, 2010). Hydrology observations indicated that the subsurface flow on the north slope of the subalpine meadow accounted for 94.5% of the total runoff in the Qinghai Lake Basin (Hu et al., 2020). In brief, precipitation is probably converted into runoff mainly in the form of lateral subsurface flow through the organic layer in alpine wetlands from early May to late October in the investigated SCG permafrost basin (Fig. 8).

From mid-April to late May, the active layer thawed at a shallow depth. When heavy and continuous precipitation occurs, the soils of the thawed layer in alpine wetlands rapidly approach saturated. With the permafrost as an aquitard, rapid runoff will occur on the slope of alpine wetlands, including subsurface flows and surface/overland (in alpine wetlands close to the stream). In late autumn to late winter, as fountains and groundwater recharge streams, fountains and groundwater usually overflow the ground surface due to ground freezing, and shortly, the ground freezes up to form aufeis (Zhou et al., 2007). The melting aufeis also affect the runoff processes in the spring season, as reported in the Colville River basin on the North Slope of Alaska (Walker and Hudson, 2003). Consequently, the heavy and continuous precipitation as well as the aufeis/icing and/or ground ice meltwater quickly replenish the stream in the forms of surface and subsurface flows, forming the spring floods.

From mid-May to mid-September, precipitation mainly infiltrates as subsurface flow (especially preferential flow) (Woo and Marsh, 2005), replenishing soil moisture, supra-permafrost water and groundwater in the deep aquifer, in addition to vegetation interception and evapotranspiration consumption (Fig. 8). The VWC at depths of 0−20 cm showed severe fluctuations due to rainfall events (Fig. 5a and c). With the plant roots of alpine meadows being primarily concentrated in the organic horizon at depths of 0−20 cm (Yue et al., 2015; Zhou et al., 2005), higher SHC of the organic horizon led to soil preferential flow to quickly replenish the soil water close to the root zone (Quinton and Marsh et al., 1998; Woo and Marsh, 2005). Additionally, increased transpiration during the growing season improved root water retention. As the active layer gradually thawed from top down, the storage capacity of the basin increased, and the runoff at the basin outlet notably declined in late May and early June (Fig. 2b). From early June to September, the northeastern QTP experienced a rainy season, and the soil VWC of alpine wetlands was high as a result (Fig. 5a and c). From mid-September to late October, the active layer gradually approached its maximum thaw depth in alpine wetlands, with the VWC close to saturation at depths of 0−73 cm (Fig. 5c). When heavy and continuous rainfall occurs, runoff occurs rapidly on the slopes of alpine wetlands and quickly recharges the stream, especially through subsurface flows, resulting in the autumn floods (Fig. 2b, 5a and 5c, and 8). In mid-to late October, the active layer began to refreeze. As liquid water freezes into ground ice, the volume of the active layer expands, subsequently squeezing the space between soil pores (Cheng et al., 2017). Under certain conditions, the freezing front can move like a piston, and the bi-directional ground freezing will accelerate the drainage of the partial or full artesian supra-permafrost water (Cheng et al., 2017). This may also increase runoff at the basin outlet to some extent.

6. Conclusions

(1) Unlike the seasonal frost regions, the runoff curve in the SCG permafrost basin in the HAYR exhibited a bimodal distribution, *i.e.*, spring and autumn floods. Spring flood in mid-April to late May is mainly due to heavy and continuous precipitation as well as the aufeis/icing meltwater, while autumn flood in mid-September to late October is caused by heavy and continuous rainfall.
(2) The high ratio of annual evapotranspiration to precipitation (>1.0) in the investigated wetland is mainly due to the considerably underestimated 'observed' precipitation caused by the wind-induced instrumental error and the neglect of snow sublimation. Except the enhanced water storage in the wetland ecosystem in June, August and September, it was all deficient in other months during the investigated periods.
(3) The stream runoff from early May to late October probably comes from the lateral discharge of subsurface flow in alpine wetlands in the investigated SCG permafrost basin.

Declaration of competing interest

The authors declare that they have no known competing financial interests or personal relationships that could have appeared to influence the work reported in this paper.

Acknowledgments

This study is supported by the Natural Science Foundation of China (41971091) and Autonomous Province of Bozen/Bolzano − Department for Innovation, Research and University in the frame of the International Mobility for Researchers Programme (13585/2023).

References

An, Z., Kutzbach, J.E., Prell, W.L., et al., 2001. Evolution of Asian monsoons and phased uplift of the Himalaya−Tibetan Plateau since late miocene times. Nature 411, 62−66. https://doi.org/10.1038/35075035.

Bense, V.F., Kooi, H., Ferguson, G., et al., 2012. Permafrost degradation as a control on hydrogeological regime shifts in a warming climate. J. Geophys. Res. Earth Surf. 117, F03036.

Chen, D., Xu, B., Yao, T., et al., 2015. Assessment of past, present and future environmental changes on the Tibetan Plateau. Chin. Sci. Bull. 60, 3025−3035. https://doi.org/10.1360/N972014-01370 (Chinese).

Please cite this article as: WANG, Q.-F et al., Water budgets in an arid and alpine permafrost basin: Observations from the High Mountain Asia, Advances in Climate Change Research, https://doi.org/10.1016/j.accre.2024.09.005

Chen, F., Zhang, J., Liu, J., et al., 2020. Climate change, vegetation history, and landscape responses on the Tibetan Plateau during the Holocene: a comprehensive review. Quat. Sci. Rev. 243, 106444. https://doi.org/10.1016/j.quascirev.2020.106444.

Chen, R., Wang, G., Yang, Y., et al., 2018. Effects of cryospheric change on alpine hydrology: combining a model with observations in the upper reaches of the Hei River, China. J. Geophys. Res. Atmos. 123, 3414−3442. https://doi.org/10.1002/2017JD027876.

Cheng, G., Fan, J., Peng, L., 2017. Progresses in soil freezing−thawing effects on the runoff generation in plateau−mountain regions. Adv. Earth Sci. 32 (10), 1020−1029 (Chinese).

Cheng, G., Jin, H., 2013. Permafrost and groundwater on the Qinghai−Tibet Plateau and in Northeast China. Hydrogeol. J. 21, 5−23.

Chow, V.T., 1959. Open-Channel Hydraulics. McGraw-Hill, New York.

Clarke, R.T., 1999. Uncertainty in the estimation of mean annual flood due to rating curve in definition. J. Hydrol. 222 (1−4), 185−190. https://doi.org/10.1016/S0022-1694(99)00097-9.

Cuo, L., Zhang, Y., Gao, Y., et al., 2013. The impacts of climate change and land cover/use transition on the hydrology in the upper Yellow River Basin, China. J. Hydrol. 502, 37−52.

Dai, L., Fu, R., Guo, X., et al., 2021. Evaluation of actual evapotranspiration measured by large-scale weighing lysimeters in a humid alpine meadow, northeastern Qinghai−Tibetan Plateau. Hydrol. Process. 35, e14051. https://doi.org/10.1002/hyp.14051.

Ding, Y., Zhang, S., Zhao, L., Li, Z., Kang, S., 2019. Global warming weakening the inherent stability of glaciers and permafrost. Sci. Bull. 64, 245−253. https://doi.org/10.1016/j.scib.2018.12.028.

Du, F., Li, Z., Gui, J., et al., 2024. Mechanisms of suprapermafrost groundwater recharge streamflow in alpine permafrost regions: insights from young water fraction analysis. Water Resour. Res. 60, e2024WR037329.

Fenton, J.D., Keller, R.J., 2001. The calculation of streamflow from measurements of stage. Coop. Res. Cent. Catchment Hydrol. 7−37.

Gao, B., Yang, D., Qin, Y., et al., 2018. Change in frozen soils and its effect on regional hydrology, upper Heihe basin, northeastern Qinghai−Tibetan Plateau. Cryosphere 12, 657−673.

Gao, H., Han, C., Chen, R., et al., 2022. Frozen soil hydrological modeling for a mountainous catchment northeast of the Qinghai−Tibet Plateau. Hydrol. Earth Syst. Sci. 26, 4187−4208. https://doi.org/10.5194/hess-26-4187-2022.

Gao, H., Wang, J., Yang, Y., et al., 2021. Permafrost hydrology of the Qinghai−Tibet Plateau: a review of processes and modeling. Front. Earth Sci. 8, 576838. https://doi.org/10.3389/feart.2020.576838.

Grünberg, I., Wilcox, E.J., Zwieback, S., et al., 2020. Linking tundra vegetation, snow, soil temperature, and permafrost. Biogeosciences 17, 4261−4279. https://doi.org/10.5194/bg-17-4261−2020.

He, H.L., He, D., Jin, J.M., et al., 2020. Room for improvement: a review and evaluation of 24 soil thermal conductivity parameterization schemes commonly used in land-surface, hydrological, and soil-vegetation-atmosphere transfer models. Earth Sci. Rev. 103419. https://doi.org/10.1016/j.earscirev.2020.103419.

Hinkel, K.M., Paetzold, F., Nelson, F.E., et al., 2001. Patterns of soil temperature and moisture in the active layer and upper permafrost at Barrow, Alaska: 1993−1999. Global Planet. Change 29, 293−309.

Hu, G.R., Li, X.Y., Yang, X.F., 2020. The impact of micro-topography on the interplay of critical zone architecture and hydrological processes at the hillslope scale: integrated geophysical and hydrological experiments on the Qinghai−Tibet Plateau. J. Hydrol. 583, 124618.

Immerzeel, W.W., Lutz, A.F., Andrade, M., et al., 2020. Importance and vulnerability of the world's water towers. Nature 577, 364−369. https://doi.org/10.1038/s41586-019-1822-y.

Jin, H., He, R., Cheng, G., et al., 2009. Changes in frozen ground in the source area of the Yellow River on the Qinghai−Tibet Plateau, China, and their eco-environmental impacts. Environ. Res. Lett. 4, 045206. https://doi.org/10.1088/1748-9326/4/4/045206.

Jin, H., Huang, Y., Bense, V.F., et al., 2022. Permafrost degradation and its hydrogeological impacts. Water 14 (3), 372. https://doi.org/10.3390/w14030372.

Jin, H., Li, S., Cheng, G., et al., 2000. Permafrost and climatic change in China. Global Planet. Change 26, 387−404.

Kumar, A., 2011. Stage-discharge relationship. In: Singh, V.P., Singh, P., Haritashya, U.K. (Eds.), Encyclopedia of Snow, Ice, and Glaciers. Springer, Dordrecht, pp. 1079−1081. https://doi.org/10.1007/978-90-481-2642-2.

Koch, J.C., Connolly, C.T., Baughman, C., 2024. The dominance and growth of shallow groundwater resources in continuous permafrost environments. Proc. Natl. Acad. Sci. U.S.A. 121 (23), e2317873121. https://doi.org/10.1073/pnas.2317873121.

Lambie, J.C., 1978. Measurement of flow: velocity-area methods. In: Herschy, R.W. (Ed.), Hydrometry: Principles and Practices. John Wiley, Chichester, pp. 1−52.

Li, J., Sheng, Y., Wu, J., et al., 2016. Landform-related permafrost characteristics in the source area of the Yellow River, eastern Qinghai−Tibet Plateau. Geomorphology 269, 104−111. https://doi.org/10.1016/j.geomorph.2016.06.024.

Li, X., Che, T., Li, X., et al., 2020a. CAS Earth poles: big data for the three poles. Bull. Am. Meteorol. Soc. 101 (9), E1475−E1491. https://doi.org/10.1175/BAMS-D-19-0280.1.

Li, Z., Li, Z., Feng, Q., et al., 2020b. Runoff dominated by supra-permafrost water in the source region of the Yangtze river using environmental isotopes. J. Hydrol. 582, 124506.

Li, X., Cheng, G., Jin, H., et al., 2008. Cryospheric change in China. Global Planet. Change 62, 210−218. https://doi.org/10.1016/j.gloplacha.2008.02.001.

Li, Z., Feng, Q., Liu, W., et al., 2014. Study on the contribution of cryosphere to runoff in the cold alpine basin: a case study of Hulugou River basin in the Qilian Mountains. Global Planet. Change 122, 345−361.

Li, Z., Gui, J., Cui, Q., et al., 2024. Soil water sources and their implications for vegetation restoration in the Three-Rivers Headwater region during different ablation periods. Hydrol. Earth Syst. Sci. 28, 719−734. https://doi.org/10.5194/hess-28-719-2024.

Lindström, G., Bishop, K., Lofvenius, M.O., 2002. Soil frost and runoff at Svartberget, northern Sweden: measurements and model analysis. Hydrol. Process. 16, 3379−3392. https://doi.org/10.1002/hyp.1106.

Lischeid, G., 2008. Combining hydrometric and hydrochemical data sets for investigating runoff generation processes: tautologies, inconsistencies and possible explanations. Geogr. Compass. 2 (1), 255−280.

Liston, G.E., Sturm, M., 2004. The role of winter sublimation in the Artic moisture budget. Nord. Hydrol 35 (4−5), 325−334. https://doi.org/10.2166/nh.2004.0024.

Liu, X.N., Mo, L.J., Xin, Y.H., et al., 2024. Research on the temporal and spatial variations of snow cover and snowline altitude in the Tibetan Plateau region. Journal of North China University of Water Resources and Electric Power (Natural Science Edition) 45 (2), 48−58 (Chinese).

Lopez, C.M.L., Brouchkov, A., Nakayama, H., et al., 2010. Epigenetic salt accumulation and water movement in the active layer of central Yakutia in eastern Siberia. Hydrol. Process. 21 (1), 103−109.

Loukas, A., Vasiliades, L., 2014. Streamflow simulation methods for ungauged and poorly gauged watersheds. Nat. Hazards Earth Syst. Sci. 14, 1641−1661.

Luo, D., Jin, H., Jin, X., et al., 2018. Elevation-dependent thermal regime and dynamics of frozen ground in the bayan har mountains, northeastern Qinghai−Tibet Plateau, Southwest China. Permafr. Periglac. Process 29, 257−270. https://doi.org/10.1002/ppp.1988.

Ma, Q., Jin, H., Bense, V.F., et al., 2019. Impacts of degrading permafrost on streamflow in the source area of Yellow River on the Qinghai−Tibet Plateau, China. Adv. Clim. Change Res. 10 (4), 225−239. https://doi.org/10.1016/j.accre.2020.02.001.

Ma, R., Sun, Z., Chang, Q., et al., 2021. Control of the interactions between stream and groundwater by permafrost and seasonal frost in an alpine catchment, northeastern Tibet Plateau. China. J. Geophys. Res. Atmos. 126 (5), e2020JD033689. https://doi.org/10.1029/2020jd033689.

Ma, Y., Xie, Z., Chen, Y., et al., 2024. Dataset of spatially extensive long-term quality-assured land−atmosphere interactions over the Tibetan Plateau. Earth Syst. Sci. Data 16, 3017−3043. https://doi.org/10.5194/essd-16-3017-2024.

Manfreda, S., Pizarro, A., Moramarco, T., et al., 2020. Potential advantages of flow-area rating curves compared to classic stage-discharge-relations. J. Hydrol. 585, 124752.

Please cite this article as: WANG, Q.-F et al., Water budgets in an arid and alpine permafrost basin: Observations from the High Mountain Asia, Advances in Climate Change Research, https://doi.org/10.1016/j.accre.2024.09.005

McClelland, J.W., Holmes, R.M., Peterson, B.J., et al., 2004. Increasing river discharge in the Eurasian Arctic: consideration of dams, permafrost thaw, and fires as potential agents of change. J. Geophys. Res. Atmos. 109, D18102.

McGuire, K.J., McDonnell, J.J., 2010. Hydrological connectivity of hillslopes and streams: characteristic time scales and nonlinearities. Water Resour. Res. 46, W10543.

Miao, C.Y., Immerzeel, W.W., Xu, B.Q., et al., 2024. Understanding the Asian Water Tower requires a new precipitation observation strategy. Proc. Natl. Acad. Sci. U.S.A. 121 (23), e2403557121. https://doi.org/10.1073/pnas.2403557121.

Mosley, M.P., McKerchar, A.I., 1993. Streamflow. In: Maidment, D.R. (Ed.), Handbook of Hydrology. McGraw-Hill, Inc., New York, pp. 8.1−8.35.

Pan, Z., Ma, R., Sun, Z., et al., 2022. Integrated hydrogeological and hydrogeochemical dataset of an alpine catchment in the northern Qinghai−Tibet Plateau. Earth Syst. Sci. Data 14 (5), 2147−2165. https://doi.org/10.5194/essd-14-2147-2022.

Priestley, C.H.B., Taylor, R.J., 1972. Assessment of surface heat-flux and evaporation using large-scale parameters. Mon. Weather Rev. 100 (2), 81−92. https://doi.org/10.1175/1520-0493(1972)100<0081:OTAOSH>2.3.CO;2.

Quinton, W.L., Gray, D.M., Marsh, P., 2000. Subsurface drainage from hummock-covered hillslopes in the Arctic tundra. J. Hydrol. 237, 113−125.

Quinton, W.L., Hayashi, M., Pietroniro, A., 2003. Connectivity and storage functions of channel fens and flat bogs in northern basins. Hydrol. Process. 17, 3665−3684.

Quinton, W.L., Marsh, P., 1998. The influence of mineral earth hummock on subsurface drainage in the continuous permafrost zone. Permafr. Periglac. Process. 9, 213−228.

Ran, Y., Li, X., Cheng, G., et al., 2021. Mapping the permafrost stability on the Tibetan Plateau for 2005−2015. Sci. China Earth Sci. 64 (1), 62−79.

Rojas, M., Quintero, F., Young, N., 2020. Analysis of stage−discharge relationship stability based on historical ratings. Hydrology (31). https://doi.org/10.3390/hydrology7020031.

Ruehlmann, J., Köschens, M., 2009. Calculating the effect of soil organic matter concentration on soil bulk density. Soil Sci. Soc. Am. J. 73 (3), 876−885. https://doi.org/10.2136/sssaj2007.0149.

Schoeneberger, P.J., Wysocki, D.A., Benham, E.C., 2021. Soil survey staff. In: Field Book for Describing and Sampling Soils, Version 3.0. Natural Resources Conservation Service, Lincoln, NE USA.

Shanley, J.B., Chalmers, A., 1999. The effect of frozen soil on snowmelt runoff at Sleepers River, Vermont. Hydrol. Process. 13, 1843−1857. https://doi.org/10.1002/(SICI)1099-1085(199909)13:12/13<1843::AID-HYP879>3.0.CO;2-G.

Sheng, Y., Ma, S., Cao, W., et al., 2020. Spatiotemporal changes of permafrost in the headwater area of the Yellow River under a changing climate. Land Degrad. Dev. 31, 133−152.

Shur, Y.L., Jorgenson, M.T., 2007. Patterns of permafrost formation and degradation in relation to climate and ecosystems. Permafr. Periglac. Process. 18 (1), 7−19.

SSS (Soil Survey Staff), 2014. Keys to Soil Taxonomy, twelfth ed. USDA-Natural Resources Conservation Service, Washington, DC.

Song, C., Wang, G., Sun, X., et al., 2021. River runoff components change variably and respond differently to climate change in the Eurasian Arctic and Qinghai−Tibet Plateau permafrost regions. J. Hydrol. 601, 126653. https://doi.org/10.1016/j.jhydrol.2021.126653.

Song, P., Liu, G., 2021. Partitioning solid and liquid precipitation over the Tibetan Plateau based on satellite radar observations. J. Hydrometeorol. 22, 2861−2875.

Spence, C., Woo, M.K., 2003. Hydrology of subarctic Canadian Shield: soil-filled valleys. J. Hydrol. 279, 151−166.

Tong, Y., Wang, P., Li, X., et al., 2018. Water budget and evapotranspiration partition in an alpine meadow ecosystem in the upstream of the Heihe River, China. Acta Ecol. Sin. 38 (20), 7400−7411 (Chinese).

Walker, H.J., Hudson, P.F., 2003. Hydrologic and geomorphic processes in the Colville River delta, Alaska. Geomorphology 56, 291−303.

Walvoord, M.A., Kurylyk, B.L., 2016. Hydrologic impacts of thawing permafrost: a review. Vadose Zone J. 15, 1−20.

Wang, Q., Jin, H., Wu, Q., et al., 2022a. The vertical distribution of soil organic carbon and nitrogen in a permafrost-affected wetland on the Qinghai−Tibet Plateau: implications for holocene development and environmental change. Permafr. Periglac. Process. 33 (3), 286−297. https://doi.org/10.1002/ppp.2146.

Wang, Q., Jin, H., Yuan, Z., et al., 2022b. Synergetic variations of active layer soil water and salt in a permafrost-affected meadow in the headwater area of the Yellow River, northeastern Qinghai−Tibet Plateau. Int. Soil Water Conse. Res. 10, 284−292. https://doi.org/10.1016/j.iswcr.2021.08.004.

Wang, Q., Jin, H., Wu, Q., et al., 2020a. A 7-ka climatic variability record inferred from peat bog sediments in the north of Bayan Har Mountains, northeastern Tibetan Plateau. Environ. Earth Sci. 79, 156. https://doi.org/10.1007/s12665-020-8897-5.

Wang, G., Lin, S., Hu, Z., et al., 2020b. Improving actual evapotranspiration estimation integrating energy consumption for ice phase change across the Tibetan Plateau. J. Geophys. Res. Atmos. 125, e2019JD031799. https://doi.org/10.1029/2019JD031799.

Wang, G., Liu, G., Li, C., et al., 2012a. The variability of soil thermal and hydrological dynamics with vegetation cover in a permafrost region. Agr. For. Meteorol. 162−163, 44−57.

Wang, G., Mao, T., Chang, J., et al., 2017a. Processes of runoff generation operating during the spring and autumn seasons in a permafrost catchment on semi-arid plateaus. J. Hydrol. 550 (Suppl. C), 307−317. https://doi.org/10.1016/j.jhydrol.2017.05.020.

Wang, K., Zhang, T., Yang, D., 2021. Permafrost dynamics and their hydrologic impacts over the Russian Arctic drainage basin. Adv. Clim. Change Res. 12 (4), 482−498. https://doi.org/10.1016/j.accre.2021.03.014.

Wang, Q., Jin, H., Wen, J., et al., 2019a. Hydro-meteorological influences on the growing season CO_2 exchange of an alpine meadow in the northeastern Tibetan Plateau permafrost region: observations using eddy covariance method. Theor. Appl. Climatol. 138, 1063−1073. https://doi.org/10.1007/s00704-019-02861-5.

Wang, L., He, X., Ding, Y., 2019b. Characteristics and influence factors of the evapotranspiration from alpine meadow in central Qinghai−Tibet Plateau. J. Glaciol. Geocryol. 41 (4), 801−808 (Chinese).

Wang, S.T., Sheng, Y., Cao, W., et al., 2017b. Estimation of permafrost ice reserves in the source area of the Yellow River using landform classification. Adv. Water Sci. 28 (6), 801−810 (Chinese).

Wang, T., Shi, Y., Guo, D., 2012b. Frozen Ground Map of China Based on a Map of the Glaciers, Frozen Ground and Deserts in China (1981−2006). National Tibetan Plateau/Third Pole Environment Data Center doi: CSTR:18406.11.Geocry.tpdc.270038.

Wang, T., Yang, D., Yang, Y., et al., 2023. Pervasive permafrost thaw exacerbates future risk of water shortage across the Tibetan Plateau. Earth's Future 11 (10), e2022EF003463.

Wani, J.M., Thayyen, R.J., Ojha, C.S.P., et al., 2021. The surface energy balance in a cold and arid permafrost environment, Ladakh, Himalayas, India. Cryosphere 15, 2273−2293.

WMO (World Meteorological Organization), 2010. Manual on Stream Gauging, Volume II: Computation of Discharge. No. 1044.

Woo, M.K., 2012. Permafrost Hydrology. Springer-Verlag, Berlin Heidelberg.

Woo, M.K., Marsh, P., 2005. Snow, frozen soils and permafrost hydrology in Canada, 1999−2002. Hydrol. Process. 19, 215−229.

Xiao, J., Wang, G., Hu, Z., et al., 2023. Application evaluation of evapotranspiration models for an alpine meadow in permafrost region: a case study of Fenghuoshan area on the Qinghai−Tibet Plateau. J. Glaciol. Geocryol. 45 (3), 1−11 (Chinese).

Xiao, X., Zhang, F., Che, T., et al., 2020. Changes in plot-scale runoff generation processes from the spring−summer transition period to the summer months in a permafrost-dominated catchment. J. Hydrol. 587, 124966.

Yamanakaa, T., Kaihotsub, I., Oyunbaatarc, D., et al., 2007. Summertime soil hydrological cycle and surface energy balance on the Mongolian steppe. J. Arid Environ. 69, 65−79.

Yang, D., Kane, D.L., 2021. Arctic Hydrology, Permafrost and Ecosystems. Springer, Berlin.

Please cite this article as: WANG, Q.-F et al., Water budgets in an arid and alpine permafrost basin: Observations from the High Mountain Asia, Advances in Climate Change Research, https://doi.org/10.1016/j.accre.2024.09.005

Yang, K., Wu, H., Qin, J., et al., 2014. Recent climate changes over the Tibetan Plateau and their impacts on energy and water cycle: a review. Global Planet. Change 112, 79−91. https://doi.org/10.1016/j.gloplacha.2013.12.001.

Yang, Y., Guo, X., Wu, Q., et al., 2023. Formation processes of shallow ground ice in permafrost in the Northeastern Qinghai−Tibet Plateau: a stable isotope perspective. Sci. Total Environ. 863, 160967.

Yang, Z., Yang, Z., Wang, Q., 1992. Runoff analysis and estimation of the Binggou basin in the Qilian Mountains. J. Glaciol. Geocryol. 14 (3), 251−257 (Chinese).

Yang, F., Zhang, G.-L., Yang, J.-L., et al., 2014. Organic matter controls of soil water retention in an alpine grassland and its significance for hydrological processes. J. Hydrol. 519, 3086−3093.

Yao, T., Bolch, T., Chen, D., et al., 2022. The imbalance of the Asian water tower. Nat. Rev. Earth Environ. 3 (10), 618−632, 2022.

Yao, T., Xue, Y., Chen, D., et al., 2019a. Recent Third Pole's rapid warming accompanies cryospheric melt and water cycle intensification and interactions between monsoon and environment: multi-disciplinary approach with observation, modeling and analysis. Bull. Am. Meteorol. Soc. 100 (3), 423−444.

Yao, T., Wu, G., Xu, B., et al., 2019b. Asian water tower change and its impacts. Bull. Chin. Acad. Sci. 234 (11), 1203−1209 (Chinese).

Ye, B., Yang, D., Ding, Y., et al., 2004. A bias-corrected precipitation climatology for China. J. Hydrometeorol. 5, 1147−1160.

Ye, B., Yang, D., Zhang, Z., et al., 2009. Variation of hydrological regime with permafrost coverage over Lena Basin in Siberia. J. Geophys. Res. Atmos. 114, D07102.

Yi, P., Wan, C., Jin, H., et al., 2018. Hydrological insights from hydrogen and oxygen isotopes in source area of the Yellow River, east-northern part of Qinghai−Tibet Plateau. J. Radioanal. Nucl. Chem. 317 (1), 131−144.

Yin, Y.H., Wu, S.H., Zhao, D.S., et al., 2016. Ecosystem water conservation changes in response to climate change in the Source Region of the Yellow River from 1981 to 2010. Geogr. Res. 35 (1), 49−57 (Chinese).

You, Q., Xue, X., Peng, F., et al., 2017. Surface water and heat exchange comparison between and bare land in a permafrost region of the Tibetan Plateau. Agric. For. Meteorol. 232, 48−65.

Yue, G., Zhao, L., Wang, Z., et al., 2015. Relationship between alpine meadow root distribution and active layer temperature variation in permafrost areas. J. Glaciol. Geocryol. 37 (5), 1381−1387 (Chinese).

Zeng, C., Zhang, F., Wang, Q.J., et al., 2013. Impact of alpine meadow degradation on soil hydraulic properties over the Qinghai−Tibetan Plateau. J. Hydrol. 478, 148−156. https://doi.org/10.1016/j.jhydrol.2012.11.058.

Zhang, W., Wang, G., Hu, Z., 2023a. Comparison of three evapotranspiration calculation methods: a case study of Fenghuoshan area on the Qinghai−Tibet Plateau. J. Glaciol. Geocryol. 45 (1), 130−139 (Chinese).

Zhang, F., Li, H., Wang, W., et al., 2018a. Net radiation rather than surface moisture limits evapotranspiration over a humid alpine meadow on the northeastern Qinghai−Tibetan Plateau. Ecohydrology 11, e1925.

Zhang, G., Yang, F., Long, H., 2023b. Save the life-sustaining mattic layer on the Qinghai−Tibetan Plateau. Innovation 4 (3), 100418.

Zhang, Y., Cheng, G., Li, X., et al., 2018b. Influences of frozen ground and climate change on hydrological processes in an alpine watershed: a case study in the upstream area of the Hei'he River, Northwest China. Permafr. Periglac. Process. 28 (2), 420−432. https://doi.org/10.1002/ppp.1928.

Zhang, Z., Li, M., Wu, Q., et al., 2024. Degradation and local growth of "Xing'an-Baikal" permafrost responding to climate warming and the consequences. Earth Sci. Rev. 104865. https://doi.org/10.1016/j.earscirev.2024.104865.

Zhao, L., Cheng, G., Li, S., et al., 2000. Thawing and freezing processes of the active layer in Wudaoliang region of Tibetan Plateau. Chin. Sci. Bull. 4 (23), 2181−2187, 2000.

Zhao, L., Hu, G., Liu, G., et al., 2024. Investigation, monitoring, and simulation of permafrost on the Qinghai−Tibet Plateau: a review. Permafr. Periglac. Process. 35, 412−422. https://doi.org/10.1002/ppp.2227.

Zheng, D., van der Velde, R., Su, Z., et al., 2018. Impact of soil freeze−thaw mechanism on the runoff dynamics of two Tibetan rivers. J. Hydrol. 563, 382−394.

Zhou, H., Zhao, X., Zhou, L., et al., 2005. A study on correlations between vegetation degradation and soil degradation in the alpine meadow of the Qinghai−Tibetan Plateau. Acta Pratacult. Siniva 14 (3), 31−40 (Chinese).

Zhou, Q., Liu, S., Li, C., 2007. Investigation of frozen soil engineering geological features along the Nagqu−Jiali Highway, Tibet. J. Glaciol. Geocryol. 29 (4), 668−670 (Chinese).

Zou, D., Zhao, L., Sheng, Y., et al., 2017. A new map of permafrost distribution on the Tibetan Plateau. Cryosphere 11 (6), 2527−2542.

Please cite this article as: WANG, Q.-F et al., Water budgets in an arid and alpine permafrost basin: Observations from the High Mountain Asia, Advances in Climate Change Research, https://doi.org/10.1016/j.accre.2024.09.005